PHYSICAL REVIEW B **84**, 060404(R) (2011)

Helical magnetic order in MnSi thin films

E. A. Karhu,[1] S. Kahwaji,[1] M. D. Robertson,[2] H. Fritzsche,[3] B. J. Kirby,[4] C. F. Majkrzak,[4] and T. L. Monchesky[1,*]

[1]*Department of Physics and Atmospheric Science, Dalhousie University, Halifax, Nova Scotia, Canada B3H 3J5*

[2]*Department of Physics, Acadia University, Wolfville, Nova Scotia, Canada B4P 2R6*

[3]*National Research Council Canada, Canadian Neutron Beam Centre, Chalk River, Ontario, Canada K0J 1J0*

[4]*Center for Neutron Research, NIST, Gaithersburg, Maryland 20899, USA*

(Received 2 June 2011; published 22 August 2011)

We present a study of the magnetic structure of crystalline MnSi(111) thin films grown by molecular beam epitaxy. A combination of polarized neutron reflectometry (PNR) and superconducting quantum interference device magnetometry show that the films have helical magnetic order with a pitch vector **Q** along the film normal. The helix wavelength of $2\pi/Q = 13.9 \pm 0.1$ nm is found to be independent of thickness below 40 nm. PNR shows that the magnetic structure has both left-handed and right-handed chiralities due to the presence of inversion domains observed by transmission electron microscopy.

DOI: 10.1103/PhysRevB.84.060404 PACS number(s): 75.25.−j, 75.30.−m, 75.70.Ak, 68.37.−d

Chiral magnetic systems present new opportunities for spintronics, and a number of predictions motivate the exploration of spin-dependent electron transport in these materials.[1,2] The recent demonstration of spin-transfer torque in bulk MnSi crystals[3] motivates a search for this effect in thin films where currents can be more easily controlled and structures can be more easily engineered than in bulk. The helical order in bulk is understood by a hierarchy of interactions.[4–6] The dominant ferromagnetic exchange energy per unit cell $\frac{A}{2S}\mathbf{S}\cdot\nabla^2\mathbf{S}$ (A is the spin wave stiffness) is destabilized by the Dzyaloshinskii-Moriya interaction (DMI) $\frac{D}{S}\mathbf{S}\cdot(\nabla\times\mathbf{S})$ (D is the Dzyaloshinskii constant) that is present due to the lack of inversion symmetry in the B20 crystal structure. The competing interactions produce helical magnetic order with an 18-nm pitch, while a weaker anisotropic exchange interaction causes the pitch vector **Q** to point along the [111] direction. The magnetic texture is sensitive to both magnetic fields and pressure.[7–9]

In thin films, changes to the magnetic structure can be expected to be brought on by finite-size effects,[10] the symmetry breaking of the interfaces, and strain, which is predicted to stabilize the skyrmion phase.[11] In our previous paper on MnSi thin films grown by solid phase epitaxy (SPE), we could not find direct evidence of helical magnetic order.[12] A measurement of the remanent magnetization M_r as a function of thickness was expected to provide a measure of the wavelength of the helix. For a helimagnetic film with an out-of-plane **Q**, the magnetic moments are expected to lie in plane and align ferromagnetically in a given layer, but spiral around the film normal. In such a film the remanent magnetization will oscillate as a function of film thickness d according to

$$M_r = f M_{\text{sat}} \frac{\sin(Qd/2)}{Qd/2}, \tag{1}$$

where f is a scaling factor and M_{sat} is the saturation magnetization. However, the M_r in our SPE samples did not follow Eq. (1), possibly due to film heterogeneities obscuring the expected oscillations, which motivated our search for smoother films in order to determine the magnetic structure. In this Rapid Communication, we present results from significant improvements in MnSi/Si interfacial roughness achieved by codeposition of Mn and Si using molecular beam epitaxy (MBE), which increased appreciably the amplitude of the oscillations in x-ray reflectometry (XRR) and polarized neutron reflectometry (PNR) measurements that enabled a direct observation of the helical order.

Our films were prepared on both high- (>5000 Ω cm) and low- (1–20 Ω cm) resistivity Si (111) wafers using the same cleaning procedure as mentioned in our previous paper.[12] We deposited a 0.5-nm Mn layer onto our substrate at room temperature and then raised the temperature until a characteristic $\sqrt{3}\times\sqrt{3}$ reflection high-energy electron diffraction (RHEED) pattern indicated that a layer of MnSi had formed.[13,14] Mn and Si were codeposited onto the MnSi seed layer at a substrate temperature of 400 °C, followed by a 20-nm-thick protective amorphous silicon cap grown at room temperature.

X-ray diffraction (XRD) measurements indicated a significant improvement in the quality of the interfaces of the MBE-grown films compared to the SPE-grown films. For SPE samples, interfacial roughness washed out the Kiessig fringes on the sides of the MnSi(111) peak for film thicknesses greater than 10.5 nm, whereas fringes were observed up to the largest thickness (39.5 nm) for MBE-grown samples. The rms roughness of a 9-nm codeposited sample was 0.5 nm, as determined by XRR, compared to 1 nm in a comparable SPE sample. However, the codeposited sample roughness varies little with thickness, whereas the SPE sample roughness increases significantly with thickness.

Since MnSi occupies a very narrow region of the Mn-Si phase diagram, this phase was sensitive to the ratio of the Mn to Si fluxes. Although the MBE samples have sharper interfaces, many of the MBE samples contain $MnSi_{1.7}$ precipitates. Plan-view and cross-sectional transmission electron microscopy (TEM) specimens were prepared by low-angle mechanical polishing and imaged with a 300-kV TEM.[15] The $MnSi_{1.7}$ precipitates were found to be up to a few hundred nm in diameter, an example of which is shown in Fig. 1. However, these precipitates showed no significant effect on the magnetic measurements owing to their low magnetic moment of $0.012\mu_B$/Mn,[16] and to their small total volume relative to

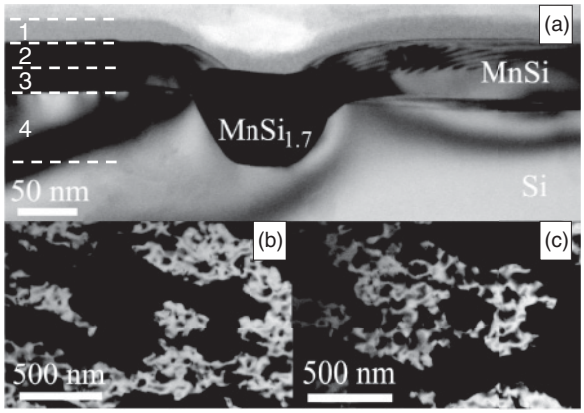

FIG. 1. (a) Cross-section bright-field TEM image of the 39.5-nm-thick MnSi film showing one of the $MnSi_{1.7}$ precipitates. (b) and (c) show plane-view TEM dark-field images of a 17.6-nm-thick film that had no precipitates. The complementary $(0\bar{1}2)$ and $(\bar{1}02)$ reflections were used in (b) and (c), respectively, which have opposite contrast for opposite crystal chiralities (Ref. 12).

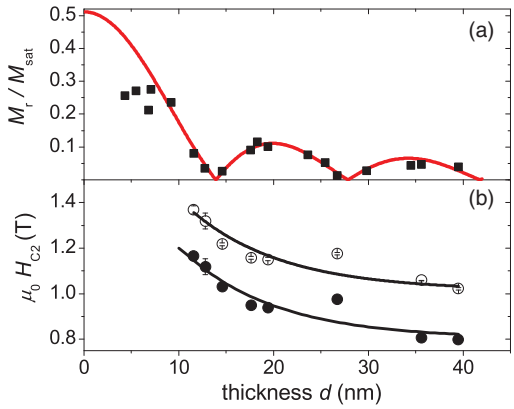

FIG. 2. (Color online) (a) The remanent magnetization at $T = 5$ K normalized to the saturation magnetization as a function of MnSi film thickness. The solid line shows the fit to the data using Eq. (1), which gives $2\pi/Q = 13.9 \pm 0.1$ nm. (b) The out-of-plane saturation field H_{C2}, measured at $T = 5$ K, is represented by open circles with $\pm 1\sigma$ error bars. The filled circles represent $H_{C2}^{\text{int}} = H_{C2} - M_{\text{sat}}$.

MnSi. We confirm this by the fact that the measured magnetic moment drops from the bulk value in proportion of the fraction of the film occupied by precipitates.

Since MnSi has a noncentrosymmetric crystal structure, there is a handedness in the crystal structure. TEM shows that both left-handed and right-handed domains are present in our films, similar to the SPE samples. We imaged the chiral domains by tilting our thin-film sample 16° from the [111] direction to the [221] zone axis of MnSi. From Figs. 1(b) and 1(c), we observe that the domains are a few hundred nm in width, compared to the micrometer-sized domains in the SPE samples. Half of the domains in the dark-field TEM micrograph of a 17.6-nm-thick MnSi film produced from the $(0\bar{1}2)$ reflection have a bright intensity, whereas the image contrast is reversed using the complementary $(\bar{1}02)$ reflection. In our previous paper we showed that the crystal structures in these two regions have opposite chiralities.[12] This has important implications for the magnetic properties since the chirality of the magnetic structure is determined by the handedness of the crystal structure.

The magnetic properties of our samples were measured with a superconducting quantum interference device (SQUID) magnetometer. The average Curie temperature $T_C = 42.3 \pm 0.2$ K for thicknesses greater than 11 nm is comparable to that found in our SPE samples and was not affected by the presence of precipitates. M_{sat} is obtained by extrapolating the magnetization data above the saturation field to zero field. Above a thickness of 10 nm, M_{sat} fluctuates about $0.42\mu_B$/Mn with a standard deviation of $0.04\mu_B$/Mn, in agreement with previous measurements.[12] The remanent magnetization shown in Fig. 2 was measured by first saturating the film in a 5-T field along the in-plane $[1\bar{1}0]$ direction at a temperature of $T = 5$ K before reducing the field to zero. No remanent magnetization is obtained for out-of-plane hysteresis loops, which indicates that the magnetic moments are in plane, as expected for a helical magnet with a **Q** pointing out of plane. Figure 2 shows that M_r/M_{sat} oscillates as a function of film thickness, in excellent agreement with Eq. (1). This provides strong evidence for helical magnetic order in our films. The solid line in Fig. 2 represents a fit with two fitting parameters: Q and f. The presence of magnetic domains expected from the presence of two chiralities in the crystal structure leads to $f = 0.51 \pm 0.02$, compared to the single domain value $f = 1$. The pitch vector $Q = 0.451 \pm 0.004$ nm^{-1} corresponds to a wavelength of $2\pi/Q = 13.9 \pm 0.1$ nm. The excellent agreement between the model and the data between $d = 7$ and 40 nm suggests that the Q does not vary significantly over this range. Curiously, the wavelength of bulk MnSi under hydrostatic pressure decreases from 18 nm at ambient pressure to 14 nm at the critical pressure $p_c = 1.5$ GPa, above which the wavelength remains constant.[9]

It is interesting to examine the out-of-plane saturation field, H_{C2}, which is related to the fundamental interactions giving rise to magnetic order. As the field is increased, the magnetic moments cant increasingly out of plane and form a conical state. The field H_{C2} that identifies the transition from a conical state to a ferromagnetic (FM) state is measured from M-H loops similar to those in Ref. 12, and is plotted in Fig. 2. The intrinsic critical field, calculated by subtracting the demagnetizing field, $H_{C2}^{\text{int}} = H_{C2} - M_{\text{sat}}$, drops with increasing thickness. In bulk MnSi, the spin wave stiffness is given by $g\mu_B\mu_0 H_{C2}^{\text{int}} \cong D^2/A$ when the small anisotropic exchange interaction contribution is neglected.[5,6] However, T_C does not vary significantly between $d = 11$ and 40 nm, suggesting that the spin wave stiffness varies little in this range of thicknesses. Furthermore, given that D of MnSi has a weak pressure dependence,[17] and D/S of $Fe_xCo_{1-x}Si$ is approximately independent of composition,[18] D in the films may have a weak strain dependence and thus explain why $Q \cong D/A$ is constant in this thickness range. This suggests that there is an additional interaction that contributes to H_{C2}. An out-of-plane uniaxial anisotropy, K_u, would be expected from the epitaxially induced out-of-plane strain, and furthermore would follow the $1/d$-like dependence of the strain.

In order to find direct evidence of the magnetic structure, we performed PNR measurements on the $d = 39.5$ nm

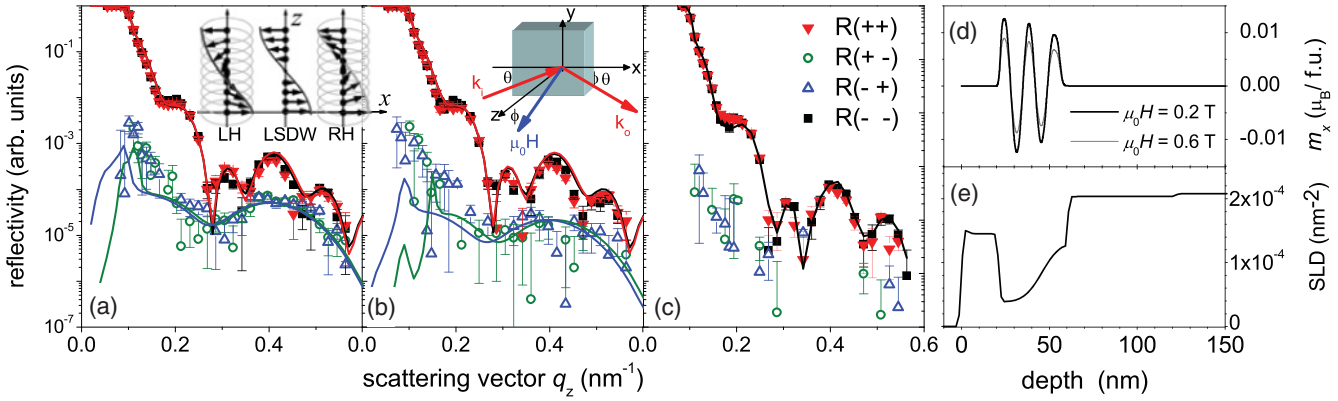

FIG. 3. (Color online) (a)–(c) PNR with $\pm 1\sigma$ error bars of a $d = 39.5$ nm MnSi film. Inset (b) shows the experimental geometry. The sample was field cooled to $T = 7$ K in a field of $\mu_0 H = 0.2$ T (a), then the field was raised to 0.6 T at $T = 7$ K (b), and finally the temperature was raised to 80 K in a field of 0.6 T (c). All four fits to the data are shown by the solid lines. A small in-plane magnetic field, created by rotating the magnetic field $\phi = 7.5^\circ$ away from the film normal, was needed to observe $R(+-)$ and $R(-+)$. (d) and (e) show the depth distribution of the magnetic moments (in units of μ_B per formula unit) and the nuclear SLD used to fit the data in (a)–(c). The magnetization profile is consistent with a linear spin-density wave (LSDW) created by a superposition of a left-handed and right-handed spin-density wave, as illustrated in inset (a).

sample using the NG-1 reflectometer at the NIST Center for Neutron Research. All four spin-dependent reflectivities $R(++)$, $R(--)$, $R(+-)$, $R(-+)$ were measured using Fe/Si supermirrors and Al-coil spin flippers to polarize and analyze the neutron spin parallel $(+)$ or antiparallel $(-)$ to the external magnetic field. To test for the existence of magnetic order, we use a nonconventional geometry where the magnetic field and the neutron spin are nearly parallel to the film normal.[18] In this geometry, the non-spin-flip reflectivities $R(++)$ and $R(--)$ are sensitive only to the chemical structure of the film, and the spin-flip channels $R(+-)$ and $R(-+)$ are sensitive to the magnetic structure and mostly independent of the chemical structure. We find from our simulations that the handedness of the chirality manifests itself as a Bragg peak in only one of the spin channels: A right-handed helix produces a peak in the down-flipped spin signal $R(+-)$, at a scattering vector $q_z = Q$, whereas for a left-handed helix, this is found in $R(-+)$.

Careful magnetic conditioning of the sample was required to observe the signatures of helical magnetic order. When we applied the field along the normal, no spin-flip signal was observed. We needed to cant the magnetic field away from the film normal to provide a small in-plane field to align the domains in the sample. The experimental geometry is shown in the inset of Fig. 3(b), where the MnSi $[1\bar{1}0]$ direction is oriented along the y axis, and the film normal points along the z axis. The field was canted in the x-z scattering plane at an angle of 7.5° with respect to the z axis. The angle was such that for $\mu_0 H = 0.2$ T, the in-plane field $H_{ip} = 26$ mT was much larger than the in-plane coercive field. Furthermore, in order to observe a peak in the spin-flip reflectivity, it was necessary to field cool the sample to a temperature $T = 7$ K in an in-plane field $\mu_0 H = 0.8$ T applied along the x axis and then rotate the field to 7.5° away from normal in order to overcome the disorder produced by the glassy magnetic behavior reported in Ref. 12. At $T = 7$ K and $\mu_0 H = 0.2$ T, there is a peak at the spin-flip signal at $q = 0.45$ nm^{-1} in Fig. 3(a). To confirm the magnetic origin of this peak, we measured the reflectivity with $\mu_0 H = 0.6$ T, which is expected to induce a conical magnetic structure with its spins canted at an angle $\alpha = \cos^{-1}(H/H_{C2}) = 54^\circ$ with respect to the film normal. As expected, the increase in external field produces the drop in the spin-flip reflectivity shown in Fig. 3(b). As a final control, we measured PNR after warming the sample to $T = 80$ K, well above T_C, in the same $\mu_0 H = 0.6$ T field, which caused the spin-flip signal to disappear altogether in Fig. 3(c).

We determine the chemical structure by simultaneously fitting the $T = 80$ K non-spin-flip PNR data and the XRR data with a common model. Given that PNR and XRR average the scattering length density (SLD) in the plane of the sample over a region with dimensions of the order of the coherence length, which are much larger than the $MnSi_{1.7}$ precipitates, the TEM image in Fig. 1(a) suggests that four individual layers, labeled 1–4, plus the substrate are required to model the reflectivities. The layers 2–4 containing Mn are modeled with four fitting parameters each: the atomic density, the atomic fraction of Mn atoms, the layer thickness, and the layer roughness. The

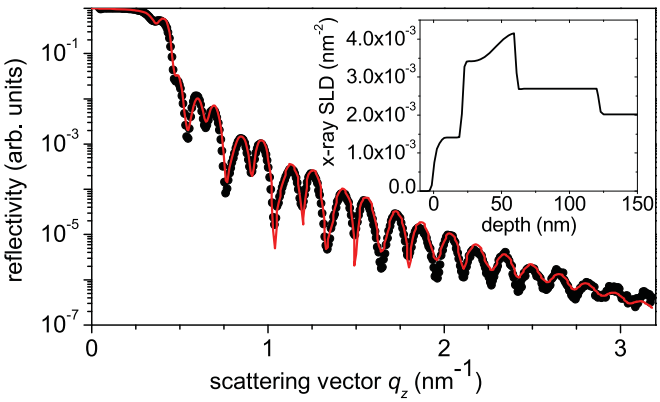

FIG. 4. (Color online) XRR for the $d = 39.5$ nm MnSi film, where the solid line corresponds to a fit to the data. The inset shows the x-ray SLD used to fit the data.

neutron and x-ray SLD profiles generated from the same set of fit parameters produce reflectivities that are in excellent agreement with both the XRR and PNR data in Figs. 3(c) and 4.

Once the nuclear scattering length density is known, the magnetic structure is obtained from the spin-flip signals. Since $R(+-) = R(-+)$, we conclude that we have both left- and right-handed magnetic chiralities in equal fractions, as expected from the TEM images. Since the coherence length of the neutrons ($\sim$10 μm) is large relative to the domain size shown in Fig. 1, the neutron reflectivity signal averages over many inversion domains with opposite magnetic chiralities. Averaging left- and right-handed helical spin density waves (SDWs) produces a linear SDW that is polarized along the in-plane component of the magnetic field, as illustrated in the inset of Fig. 3(a). The depth profile of the magnetic moments shown in Fig. 3(d) is determined from fits to the spin-flip reflectivities using only two fitting parameters: Q and the magnetic moment per formula unit. The small drop in the amplitude of the magnetic moment accounts for the drop in the MnSi concentration in layer 3 due to precipitates. The fitted wavelength $2\pi/Q = 14.0 \pm 0.5$ nm is in excellent agreement with the fit shown in Fig. 2. The lower magnetic moment than the $0.2\mu_B$ per formula unit expected from the $\mu_0 H = 0.2$ T data is explained by residual disorder that is not quenched by the in-plane component of the magnetization.

In conclusion, MnSi films on Si (111) have helical magnetic order, where the easy axis for **Q** is along the [111] direction. This order is broken into domains with both left-handed and right-handed chirality. The results from PNR measurements together with the observed oscillations in M_r demonstrate that the helical order has a constant wavelength of $2\pi/Q = 13.9 \pm 0.1$ nm in the thickness range $d = 7-40$ nm.

This work was supported by NSERC and the Canada Research Chairs Program.

*theodore.monchesky@dal.ca

[1] J. Heurich, J. König, and A. H. MacDonald, Phys. Rev. B **68**, 064406 (2003).
[2] O. Wessely, B. Skubic, and L. Nordstrom, Phys. Rev. B **79**, 104433 (2009).
[3] F. Jonietz, S. Mühlbauer, C. Pfleiderer, A. Neubauer, W. Munzer, A. Bauer, T. Adams, R. Georgii, P. Böni, R. A. Duine, K. Everschor, M. Garst, and A. Rosch, Science **330**, 1648 (2010).
[4] P. Bak and M. H. Jensen, J. Phys. C **13**, L881 (1980).
[5] M. L. Plumer and M. B. Walker, J. Phys. C **14**, 4689 (1981).
[6] S. V. Maleyev, Phys. Rev. B **73**, 174402 (2006).
[7] Y. Ishikawa and M. Arai, J. Phys. Soc. Jpn. **53**, 2726 (1984).
[8] C. Pfleiderer, D. Reznik, L. Pintschovius, H. von Lohneysen, M. Garst, and A. Rosch, Nature (London) **427**, 227 (2004).
[9] B. Fåk, R. A. Sadykov, J. Flouquet, and G. Lapertot, J. Phys. Condens. Matter **17**, 1635 (2005).
[10] E. Weschke, H. Ott, E. Schierle, C. Schüßler-Langeheine, D. V. Vyalikh, G. Kaindl, V. Leiner, M. Ay, T. Schmitte, H. Zabel, and P. J. Jensen, Phys. Rev. Lett. **93**, 157204 (2004).
[11] A. B. Butenko, A. A. Leonov, U. K. Rößler, and A. N. Bogdanov, Phys. Rev. B **82**, 052403 (2010).
[12] E. Karhu, S. Kahwaji, T. L. Monchesky, C. Parsons, M. D. Robertson, and C. Maunders, Phys. Rev. B **82**, 184417 (2010).
[13] A. Kumar, M. Tallarida, M. Hausmann, U. Starke, and K. Horn, J. Phys. D **37**, 1083 (2004).
[14] S. Higashi, Y. Ikedo, P. Kocan, and H. Tochihara, Appl. Phys. Lett. **93**, 013104 (2008).
[15] M. D. Robertson, T. Burns, and T. Morrison, Microsc. Soc. Canada Bull. **34**, 19 (2006).
[16] A. Sulpice, U. Gottlieb, M. Affronte, and O. Laborde, J. Magn. Magn. Mater. **272-276**, 519 (2004).
[17] A. Miyake, A. Villaume, Y. Haga, G. Knebel, B. Salce, G. Lapertot, and J. Flouquet, J. Phys. Soc. Jpn. **78**, 044703 (2009).
[18] S. V. Grigoriev, V. A. Dyadkin, E. V. Moskvin, D. Lamago, T. Wolf, H. Eckerlebe, and S. V. Maleyev, Phys. Rev. B **79**, 144417 (2009).
[19] G. P. Felcher, W. Lohstroh, H. Fritzsche, M. Münzenberg, H. Maletta, and W. Felsch, Appl. Phys. Lett. **72**, 2894 (1998).